CONF-791139--2

LA-UR-79-3250

TITLE: PLUME BLIGHT VISIBILITY MODELING WITH A SIMULATED PHOTOGRAPH TECHNIQUE

AUTHOR(S): M. D. Williams, E. Treiman, M. Wecksung

SUBMITTED TO: Visibility meeting Air Pollution Control Assn.
Denver, Colorado, November, 1979

LOS ALAMOS SCIENTIFIC LABORATORY
Post Office Box 1663 Los Alamos, New Mexico 87545
An Affirmative Action/Equal Opportunity Employer

Form No. 836 R3
St. No. 2629
12/78

UNITED STATES
DEPARTMENT OF ENERGY
CONTRACT W-7405-ENG. 36

PLUME BLIGHT VISIBILITY MODELING WITH A SIMULATED PHOTOGRAPH TECHNIQUE

M. D. Williams, E. Treiman, M. Wecksung

The purpose of this paper is to describe the LASL visibility model and the results of its application to plume blight problems. The model calculates pollutant dispersion, atmospheric chemistry, and radiative transfer in plumes from industrial facilities. The principal model output is in the form of a simulated photograph that depicts a scene that has been modified by light scattering particulates and light absorbing gases.

Pollutant dispersion is described by a gaussian model with provision for multiple reflections between the ground and an elevated stable layer. The atmospheric chemistry module is a photochemical oxidant code, which includes a carbon bond model, SO_2 chemistry, gas to particle conversion and particle growth and formation. Radiative tranfer is treated with a multilayer iterative solution technique.

The procedure involves collection of a clean picture of the scene that will be altered by an industrial plume. The information on the film is then extracted by a microdensitometer using fiters appropriate to the colors blue, green, and red. The resulting digital data is modified in accordance with the results of the radiative transfer calculations and written onto film. Either slide film or color print film may be used.

The model has been applied in a number of cases. Selected examples that illustrate the importance of various visibility related parameters are presented.

Introduction

In recent years, protection of scenic resources has assumed increased importance. Before 1977, visibility did play a role in the assessment of environmental impacts in the West, where federal resources were generally required for completion of major energy projects. In some cases, visibility impacts have been identified as items of major concern in decisions governing the availability of federally controlled land, coal, water, or rights of way. For example, concern over visibility impacts was a major element in the Kaiparowits controversy[1]. Until passage of the 1977 Clean Air Act amendments, however, there were no explicit visibility constraints to energy development.

The 1977 amendments both established visibility as a value to be protected and identified a major role for the federal land manager in the assessment of potential visibility impacts. Thus the Act presented the modeling community with two major challenges: 1) to develop models capable of predicting visibility impacts and 2) to provide methods for making model outputs meaningful to the general public. In this paper, we describe one response to the twin challenges of the Clean Air Act---the LASL visibility model.

Methodology

The LASL visibility system can be thought of as having two sections. One deals with the dispersion, chemistry, and radiative tranfer; the other produces an output that displays the results in a meaningful fashion. The display system is the simulated photograph technique, which produces a set of "before" and "after" pictures as the principal output.

This technique begins with an actual photograph of the scene. Preferably the photograph is obtained under clean skies and relatively clean background conditions. The photograph is digitized and the digital data is transformed into equivalent densities for a film with the same minimum density and a unit gamma. With this procedure, the density is related to exposure by the relation:

$$D = - \log E + a_o .$$

The transformed digital data is then combined with the solutions of the radiative transfer and dispersion problems by the relation:

$$D_{new} = - \mathrm{Log} \; a\left(\frac{Tr}{a} \; 10^{-Do} + B_{sky}\right)$$

where D_{new} is the modified film density, D_o is the transformed film density, T_r is the light transmission through the plume, and B_{sky} is the additional light scattered into the line of sight by the pollutants. The factor a transforms the relative intensities provided by the radiative transfer code into equivalent exposure. It is obtained by the relation:

$$a = \frac{10^{-Dref}}{I_{ref}}$$

where I_{ref} is the relative intensity calculated by the radiative transfer code for the background sky and D_{ref} is the transformed film density corresponding to the same point.

Once the modified film densities have been obtained, the simulated picture may be displayed on a CRT. To obtain a hard copy, the CRT may be photographed or the digital data may be written directly on slide or print film.

The radiative transfer and dispersion problems are solved by a multistep process. First mie scattering theory is used to calculate light scattering properties of aerosol particles with diameters of 0.1 to 2.4 microns and indices of refraction appropriate to background and plume aerosols. The light scattering calculations are performed for wavelengths of 4500, 5500, and 6500 Å, which corresponds to blue, green, and red light. The radiative transfer in the background atmosphere is calculated from the solar-zenith angle, the size distribution of the background aerosols, and the optical depths of each of thirty layers of the atmosphere. The solution involves the iterative technique developed by Braslau and Dave[2] which calculates the Fourier coefficient of intensity. The solution provides the Fourier coefficients of the different intensities for each color and layer and the Fourier coefficient of the phase functions.

The solution to the plume radiative transfer and dispersion problem also requires a number of intermediate steps. First the chemistry and particle dynamics must be defined. Key parameters are the size distribution of the secondary aerosols and the conversion half-lives for nitric oxide to nitrogen dioxide, nitrogen oxides to nitrates, and sulfur oxides to sulfates. These parameters may be estimated from reported values in the literature or calculated from a combined particle dynamics and photochemistry code. The LASL code uses a lumped parameter approach to particle dynamics and a modified carbon bond system for the chemistry[3]. (The relevant equations are reported in the appendix.) Dilution rates are based on gaussian plume dispersion.

Once the particle size distributions and the conversion rates are known, the optical properties associated with a given concentration of precursors (SO_2 and NO_x) can be calculated as a function of travel time. The dispersion module uses gaussian dispersion with Turner[4] or TVA parameters[5] to calculate concentration at each point along the observer's line of sight. Numerical integration along the line of sight provides plume optical depths and the ratios of absorption to scattering for each wavelength.

The radiation transfer problem is solved for a series of semi-infinite planes oriented normal to the line of sight. Dave's iterative technique is used and boundary conditions are obtained from the solutions to the background problem. Some adjustments to the code are made to insure that the solution without the plume is equivalent to the solution for the background atmosphere. The end product of the radiation transfer problem is a pair of transmission and light scattering values for each color and each line of sight. The model is not restricted to single scattering situations or to two crosswind lines of sight. Furthermore, the system permits the consideration of background other than the sky.

In addition to the photograph, the model also calculates plume intensities for each color, plume transmission, and plume scattering. Chromaticity coordinates, blue-red ratios, and plume to horizon brightness are also options of this model.

Applications

We have modeled a number of situations that provide insight into important plume blight cases. These include stable flow with emissions approximating current New Source Performance Standards for coal-fired power plants for plant sizes of 500-2000 MW. We have also examined various sun angles, particulate emission rates, relative humidities, observer viewing angles, and differing backgrounds. In these cases, NO_x to NO_2 conversion rates were based on measurements made in the Southwest[6]. NO was assumed to convert to NO_2 with a half-life of 2.8 h. In addition, the maximum NO_2 concentration was limited to the background ozone concentration plus 35% of the difference between the NO_x concentration and the background ozone.

In addition to coal-fired power plant plumes, we ran simulations on a wood-burning facility in Vermont. In this instance, the capacity of the facility was expanded fiftyfold.

Results

The atmospheric chemistry model produced a number of interesting results. First of all, during stable conditions, the SO_2 to SO_4 conversion rates were quite low, generally less than 0.1% per h. However, with increased dilution along the plume edges, the conversion was more rapid and increased with further dilution. Values as high as 3% were predicted along the plume edges.

The size distributions calculated by the model were sensitive to the partitioning between condensation onto existing accumulation mode particles and formation of new particles in the condensation nuclei mode. With rapid formation of condensation mode particles, relatively smaller accumulation mode particles formed, with the result that light scattering was less than would normally be predicted.

The photographic simulation identified a number of important features including the nature of the background against which the plume is observed, facility size, the source-observer geometry, the sun-plume scattering angle, the background atmospheric conditions, and the ratio of NO_2 absorption to light scattering by particulates.

Figure 1 depicts the geometry used in many of the simulations. The plant is located 30 Km from the observer and 3 m/sec winds bring the plume centerline to within 10 Km of the observer at the center of the picture. The plume travel is angled slightly toward the observer. Figure 2 is a simulated photograph of the plume from a 2000 MW plant during TVA stable conditions. Figures 3 and 4 are simulated plumes from 1000 MW and 500 MW plants, respectively. Figure 5 depicts a 2000 MW plant with particulate emissions increased threefold. In this case, the light scattering from the particulates masks the light absorption by NO_2 with the result that the plume appears white rather than brown. Figure 6 depicts the plume from a

2000 MW plant at a different time of the day so that the sun angle is much different. On the left side of the picture, which is nearest the sun, the small angle of scattering of particulates dominates NO_2 absorption, whereas on the right side of the picture the difference in the phase functions implies diminished scattering and NO_2 absorption dominates.

Figure 7 illustrates the importance of viewer geometry in the appearance of smoke plumes. This simulated photograph represents the same situation as Fig. 2 except that the observer is much closer to the plume centerline, 3 Km instead of 10 Km. The plume is barely distinguishable because of its much more diffuse boundaries. Figure 8 depicts a plume against a dirty background. In this case, the plume disappears.

Figure 9 illustrates the importance of background. In this instance, the plume from a wood-burning plant, (corresponding to 150 MW thermal) is depicted against a wooded background. The plume is distinguishable against a dark background although it would not be distinguishable against a horizon sky.

Conclusions

We have developed a visibility model for plume blight simulations that provides a simulated photograph as an output. Model applications indicate that the appearance of smoke plumes is sensitive to observer geometry, sun angle, emissions of NO_x and particulates, atmospheric stability, and the background against which the plume is visualized. Plumes from modern coal-fired power plants are primarily visible during stable conditions as a result of NO_2 discoloration of the sky.

References

1. US Department of the Interior, National Park Service, Denver Service Center, "Analysis of Kaiparowits Power Plant Impacts on National Recreation Resources," (1976).

2. Norman Braslau and J. V. Dave, "Effect of Aerosols on the Transfer of Solar Energy Through Realistic Model Atmosphere," IBM Research Report RC 014, Palo Alto, California (1972).

3. G. Z. Whitten and H. Hogo, "Mathematical Modeling of Simulated Photochemical Smog," prepared for US Environmental Protection Agency, EPA - 600/3-77-011 (1977).

4. D. B. Turner, Workbook of Atmospheric Dispersion Estimates, US Department of Health, Education, and Welfare (1969)

5. T. L. Montgomery, W. B. Norris, F. W. Thomas, and S. B. Carpenter," A Simplified Technique Used to Evaluate Atmospheric Dispersion of Emissions from Large Power Plants," Journal of the Air Pollution Control Association, Volume 23, pp. 388-394 (1973).

6. J. A. Ogren, D. L. Blumenthal, and A. H. Vanderpol, "Oxidant Measurements on Western Power Plant Plumes," prepared by Meteorology Research Incorporated for the Electric Power Research Institute, EPRI-EA-421 (1977).

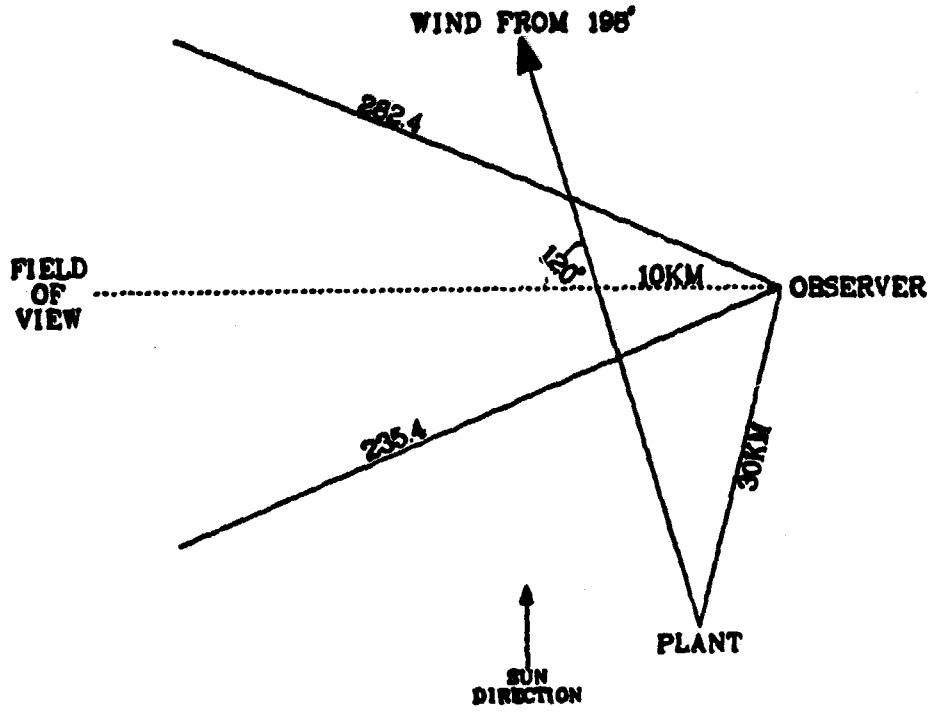

Figure 1. Source-observer geometry for the plume blight simulation.

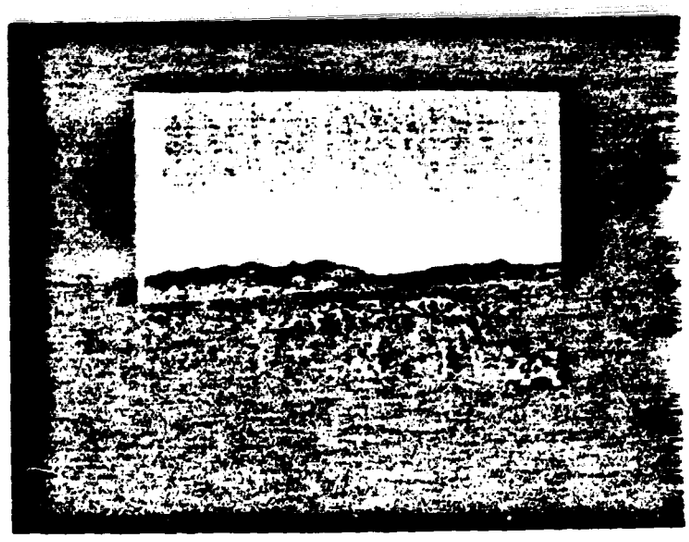

Figure 2. Simulated base case plume from a hypothetical 2000 MW coal-burning power plant.

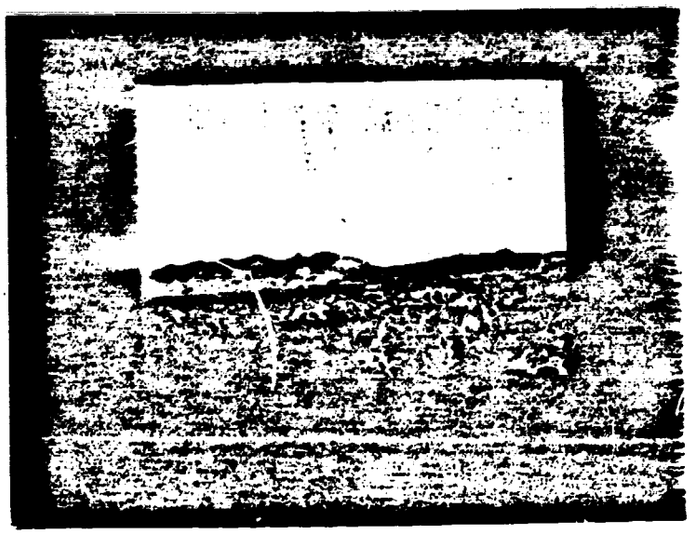

Figure 3. Simulated plume from a 1000 MW plant.

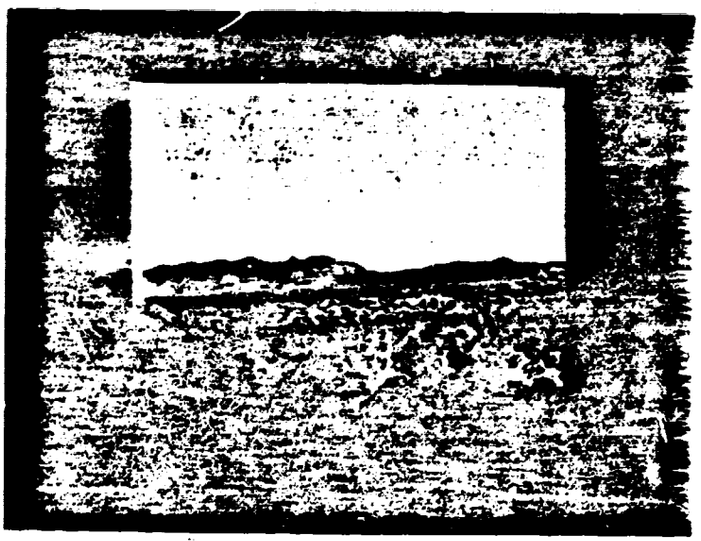

Figure 4. Simulated plume from a 500 MW plant.

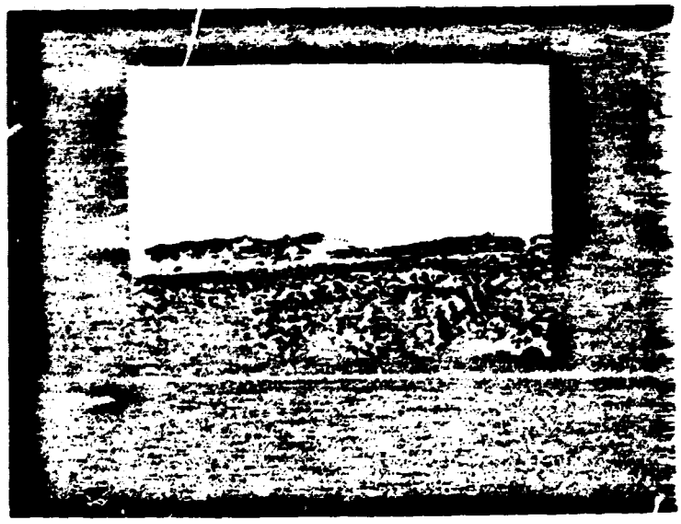

Figure 5. Simulated plume with fly ash emissions increased threefold over the base case 2000 MW plant.

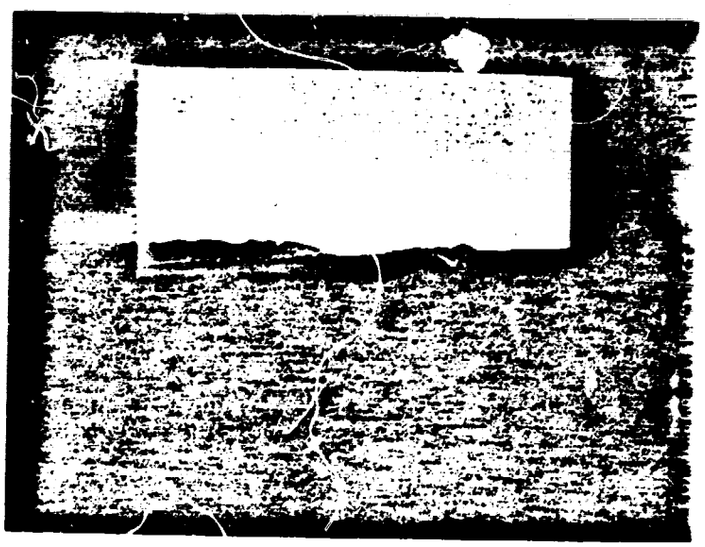

Figure 6. Simulated plume with observer looking more nearly toward the sun (scattering angle is 21^{o} vs 79^{o} for the base case).

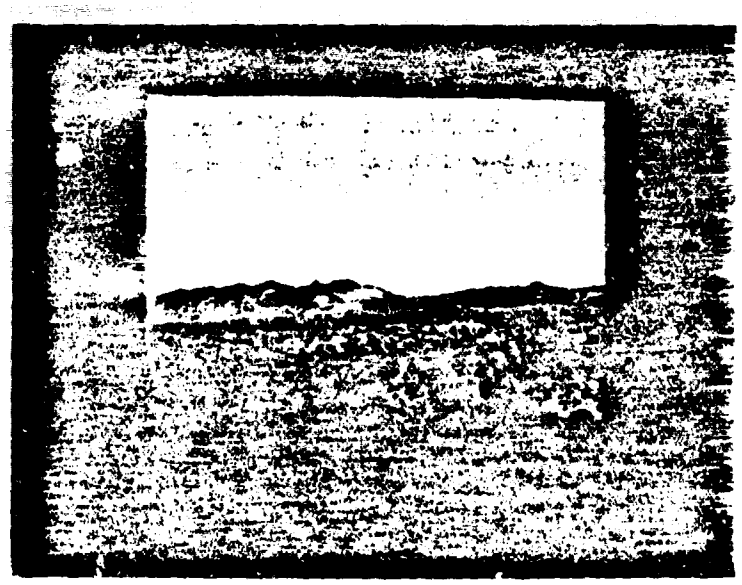

Figure 7. Simulated plume with the observer closer to the plume (3 Km instead of 10 Km in the base case) and the plume travel normal to the line of sight (orientation angle for the base case is 120^{o} rather than 90^{o}).

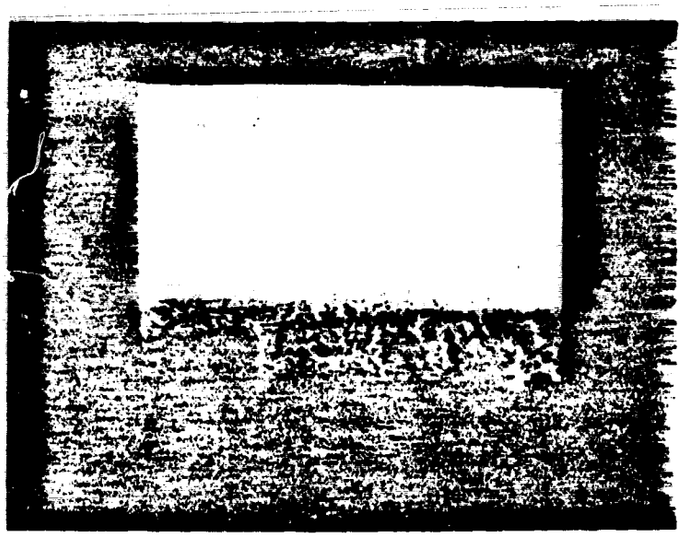

Figure 8. Simulated plume in a hazy background.

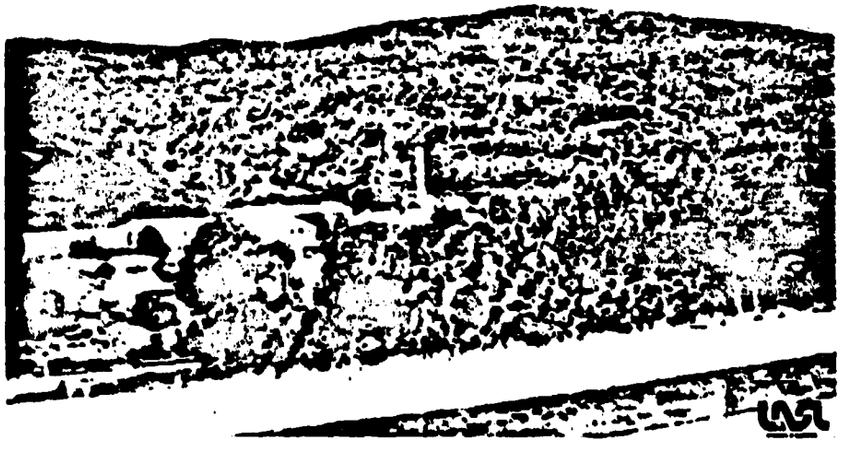

Figure 9. Simulated plume of a hypothetical 150 MW wood-burning power plant.

Appendix

Aerosol Carbon Bond Photochemical System

1)	$NO_2 + h\nu \rightarrow NO + O^{\cdot}$	$K_1 = .6\ e^{\frac{-.38}{\mu o}}\ min^{-1}$
2)	$O^{\cdot} + O_2 + M \rightarrow O_3$	$4 \times 10^6\ min^{-1}$
3)	$O3 + NO \rightarrow NO_2 + O_2$	$25.2\ ppm^{-1} min^{-1}$
4)	$2NO + O_2 \rightarrow 2NO2$	$.00015\ ppm^{-1}\ min^{-1}$
5)	$O^{\cdot} + NO_2 \rightarrow NO + O_2$	$1.34 \times 10^4\ ppm^{-1}\ min^{-1}$
6)	$O_3 + NO_2 \rightarrow NO_3 + O_2$	$.05\ ppm^{-1}\ min^{-1}$
7)	$NO_3 + NO \rightarrow 2NO_2$	$1.3 \times 10^4\ ppm^{-1}\ min^{-1}$
8)	$NO_3 + NO_2 + H_2O \rightarrow 2HNO_3$	$1.66 \times 10^{-3} \times ppm\ H_2O\ ppm^{-1}\ min^{-1}$
9)	$NO + NO_2 + H_2O \rightarrow 2HNO_2$	$2.2 \times 10^{-9} \times ppm\ H_2O\ ppm^{-1}\ min^{-1}$
10)	$HNO_2 + h\nu \rightarrow NO + OH$	$0.2 \times k_1\ min^{-1}$
11)	$NO_2 + OH^{\cdot} \rightarrow HNO_3$	$9 \times 10^3\ ppm^{-1}\ min^{-1}$
12)	$NO + OH \rightarrow HNO_2$	$9 \times 10^3\ ppm^{-1}\ min^{-1}$
13)	$CO + OH^{\cdot} \rightarrow CO_2 + HO_2^{\cdot}$	$206.\ ppm^{-1}\ min^{-1}$
14)	$OLE + OH^{\cdot} \rightarrow HCHO + CH_3O_2^{\cdot}$	$3.8 \times 10^4\ ppm^{-1}\ min^{-1}$
15)	$PAR + OH^{\cdot} \rightarrow CH_3\ O_2^{\cdot} + H_2O$	$1.3 \times 10^3\ ppm^{-1}\ min^{-1}$
16)	$ARO + OH^{\cdot} \rightarrow HCHO + CH_3O_2^{\cdot}$	$8 \times 10^3\ ppm^{-1}\ min^{-1}$
17)	$OLE + O^{\cdot} \rightarrow HC(O)O_2^{\cdot} + CH_3O2^{\cdot}$	$5.3 \times 10^3\ ppm^{-1}\ min^{-1}$

18)	$PAR + O^{\cdot} \rightarrow CH_3O_2^{\cdot} + OH^{\cdot}$	20 $ppm^{-1}\ min^{-1}$
19)	$ARO + O^{\cdot} \rightarrow HC(O)O_2^{\cdot} + CH_3O_2^{\cdot}$	37 $ppm^{-1}\ min^{-1}$
20)	$OLE + O_3 \rightarrow HC(O)O_2^{\cdot} + HCHO + OH^{\cdot}$	.01 $ppm^{-1}\ min^{-1}$
21)	$ARO + O_3 \rightarrow HC(O)O_2^{\cdot} + HCHO + OH^{\cdot}$	.002 $ppm^{-1}\ min^{-1}$
22)	$OLE + O_3 \rightarrow$ ozonide	.005 $ppm^{-1}\ min^{-1}$
23)	$HCHO + h\nu \rightarrow HC(O)O_2^{\cdot} + HO_2^{\cdot}$	$7.2 \times 10^{-4}\ k_1\ min^{-1}$
24)	$HCHO + h\nu \rightarrow CO + H_2$	$23.56 \times 10^{-4}\ k_1\ min^{-1}$
25)	$HCHO + OH^{\cdot} \rightarrow HC(O)O_2 + H_2O$	$1 \times 10^4\ ppm^{-1}\ min^{-1}$
26)	$HO_2 + NO \rightarrow OH^{\cdot} + NO2$	$2 \times 10^3\ ppm^{-1}\ min^{-1}$
27)	$CH_3O_2^{\cdot} + NO \rightarrow NO_2 + HCHO + HO_2^{\cdot}$	$2 \times 10^3\ ppm^{-1}\ min^{-1}$
28)	$HC(O)O^{\cdot} + NO \rightarrow NO_2 + CO_2 + HO_2^{\cdot}$	$2 \times 10^3\ ppm^{-1}\ min^{-1}$
29)	$H_2O_2 + h\nu \rightarrow 2OH^{\cdot}$	$.003k_1\ min^{-1}$
30)	$2\ HO_2^{\cdot} \rightarrow H_2O_2 + O_2$	$4 \times 10^3\ ppm^{-1}\ min^{-1}$
31)	$CH_3O_2^{\cdot} + HO_2 \rightarrow H_3COOH + O_2$	$4 \times 10^3\ ppm^{-1}\ min^{-1}$
32)	$HC(O)O_2 + HO_2 \rightarrow HC(O)OOH + O_2$	$1 \times 10^4\ ppm^{-1}\ min^{-1}$
33)	$HC(O)O_2 + NO_2 \rightarrow PAN$	150 $ppm^{-1}\ min^{-1}$
34)	$PAN \rightarrow HC(O)O_2 + NO_2$	.02 min^{-1}
35)	$ARO + NO_3 \rightarrow$ PRODUCTS	50. $ppm^{-1}\ min^{-1}$

36)	$HO_2^{\cdot} + NO_2 \rightarrow HNO_2$	20. $ppm^{-1}\ min^{-1}$
37)	$SO_2 + OH^{\cdot} \rightarrow SULFATE$	$1.6 \times 10^3\ ppm^{-1}\ min^{-1}$
38)	$RO_2 + SO_2 \rightarrow SULFATE + RO^{\cdot}$	$.3\ ppm^{-1}\ min^{-1}$
39)	$HO_2^{\cdot} + SO_2 \rightarrow OH^{\cdot} + SULFATE$	$1.4\ ppm^{-1}\ min^{-1}$
40)	$CH_4 + OH^{\cdot} \rightarrow CH_3O_2^{\cdot}$	$1.2 \times 10^1\ ppm^{-1}\ min^{-1}$
41)	$HNO_3 + NH_3 \rightarrow NH_4NO_3$	$.028\ ppm^{-1}\ min^{-1}$
42)	$2CN \rightarrow CN$	$CNN \times 2.277\ E\text{-}09 + 3.929 \times 10^{-1}\ \ell n\ \sigma_{gn}$ $cm^{-3}\ min^{-1}$
43)	2CN CA	W $cm^{-3}\ min^{-1}$
44)	$NH_4\ NO_3 \rightarrow \gamma CN + NH_4\ NO_3$	$1000.\ min^{-1}$
45)	$SULFATE \rightarrow \beta CN + SULFATE$	$1000.\ min^{-1}$
46)	$2CA \rightarrow CA$	$2.259 \times 10^{-10}\ (Dgna)^{-.531}\ cm^{-3}\ min^{-1}$
47)	$CA + CN \rightarrow \alpha VA$	$.0479 \times 10^{-10}\ Dgnn^{-2.3517}\ Dgsa^{B}$ $cm^{-3}\ min^{-1}$
48)	$SULFATE \rightarrow \alpha_1\ VA$	$1000.\ min^{-1}$
49)	$NH_4NO_3 \rightarrow \alpha_2\ VA$	$1000.\ min^{-1}$

ARO is aromatic

PAR is parafin

OLE is olefin